Vortex splitting in two-dimensional fluids and non-neutral electron plasmas with smooth vorticity profiles

Cite as: Phys. Plasmas **31**, 052106 (2024); doi: 10.1063/5.0201712
Submitted: 31 January 2024 · Accepted: 17 April 2024 ·
Published Online: 6 May 2024

N. C. Hurst,[1,a)] A. Tran,[2] P. Wongwaitayakornkul,[3] J. R. Danielson,[4] D. H. E. Dubin,[4] and C. M. Surko[4]

AFFILIATIONS

[1]Department of Physics, University of Wisconsin-Madison, Madison, Wisconsin 53706, USA
[2]Department of Physics and Astronomy, Michigan State University, East Lansing, Michigan 48824, USA
[3]Faculty of Science and Technology, Thammasat University, Pathum Thani 12120, Thailand
[4]Department of Physics, University of California San Diego, La Jolla, California 92093, USA

Note: This paper is part of the Special Topic: Coherent Vortical Structures in Fluids and Plasmas.
[a)]**Author to whom correspondence should be addressed:** nhurst@wisc.edu

ABSTRACT

Initially, elliptical, quasi-two-dimensional (2D) fluid vortices can split into multiple pieces if the aspect ratio is sufficiently large due to the growth and saturation of perturbations known as Love modes on the vortex edge. Presented here are experiments and numerical simulations, showing that the aspect ratio threshold for vortex splitting is significantly higher for vortices with realistic, smooth edges than that predicted by a simple "vortex patch" model, where the vorticity is treated as piecewise constant inside a deformable boundary. The experiments are conducted by exploiting the $E \times B$ drift dynamics of collisionless, pure electron plasmas in a Penning–Malmberg trap, which closely model 2D vortex dynamics due to an isomorphism between the Drift–Poisson equations describing the plasmas and the Euler equations describing ideal fluids. The simulations use a particle-in-cell method to model the evolution of a set of point vortices. The aspect ratio splitting threshold ranges up to about twice as large as the vortex patch prediction and depends on the edge vorticity gradient. This is thought to be due to spatial Landau damping, which decreases the vortex aspect ratio over time and, thus, stabilizes the Love modes. Near the threshold, asymmetric splitting events are observed in which one of the split products contains much less circulation than the other. These results are relevant to a wide range of quasi-2D fluid systems, including geophysical fluids, astrophysical disks, and drift-wave eddies in tokamak plasmas.

I. INTRODUCTION

Quasi-two-dimensional (2D) fluid dynamics is found in a variety of important natural and human-made systems, including geophysical fluids,[1] soap films,[2] astrophysical disks,[3] black hole horizons,[4] and magnetized plasmas, including fusion experiments,[5] non-neutral plasmas,[6,7] and intense charged particle beams.[8] In the case of magnetized plasmas, the magnetic field can decouple parallel and perpendicular motion, leading to fluid-like drift dynamics in the two perpendicular dimensions.[9] An important feature of 2D fluid systems is the self-organization of the vorticity into coherent, rotating structures known as vortices. Interactions between vortices in 2D can result in merger events, which contribute to the inverse turbulent cascade that drives vorticity toward large, domain-filling structures.[10] However, in some circumstances, 2D vortices can split into multiple pieces, which opposes the merger phenomenology and drives vorticity toward smaller spatial scales.[11–13] This process typically involves deformation of the vortex followed by a hydrodynamic instability that grows on its edge.

Perhaps the most well-known example of vortex splitting is that of Earth's stratospheric, arctic polar vortex, which splits on average about once every 2 years through a process known as a sudden stratospheric warming.[14] These events exchange cold, polar air with warmer air from lower latitudes, with significant consequences for the arctic environment and for life in temperate regions. They are an important

factor in global climate modeling but are difficult to predict, with some disagreement as to the rate of splitting events expected in a warming climate.[15] Interestingly, the antarctic polar vortex has split only once in recorded history, in September 2002.[16] Similar processes may be active on other planets in the solar system and beyond.[17] In tokamak magnetic fusion experiments, thermal transport is driven by drift-wave turbulence but partially suppressed due to the formation of zonal flows, analogous to the dynamics of Rossby waves in planetary atmospheres.[18] It has been suggested that the interaction of drift-wave eddies with zonal shear could result in splitting events, which could impact transport rates.[19] Vortex splitting has also been observed in quasi-2D flow across airfoils[12] and in quantum-mechanical systems such as the nonlinear Schrödinger equation[20] and Bose–Einstein condensates.[21]

These examples highlight the need to develop a basic, first-principles understanding of vortex splitting events. The simplest 2D fluid system featuring vortex dynamics is that described by the Euler equations for an ideal (inviscid and incompressible) fluid, given by

$$(\partial_t - \nabla\psi \times \hat{\mathbf{z}}\cdot\nabla)\omega = 0; \quad \nabla^2\psi = \omega, \tag{1}$$

where $\omega = \nabla \times \mathbf{v}$ is the vorticity, $\mathbf{v} = -\nabla\psi \times \hat{\mathbf{z}}$ is the fluid velocity, ψ is the stream function, and $\hat{\mathbf{z}}$ is a unit vector normal to the plane of 2D fluid motion. The problem can be further simplified by adopting a "vortex patch" model where the vorticity is taken to be piecewise constant inside a simply connected domain. Exact solutions for rotating, elliptical vortex patches were found by Kirchoff.[22,23] Waves propagating along the edge of the Kirchoff vortex were first investigated analytically by Love,[24] who found unstable modes on elliptical vortices for sufficiently large values of the aspect ratio $\lambda = a/b$, where a and b are the semimajor and semiminor axes, respectively. The most unstable wavenumber, m, becomes progressively higher as the aspect ratio increases, and in the limit of large aspect ratio, the Love instability is equivalent to the Kelvin–Helmholtz shear-layer instability. Binary vortex splitting events are associated with the growth and nonlinear saturation of $m = 4$ Love modes, whereas higher wavenumbers can result in higher-order splitting events (i.e., into more than two pieces). Analytical progress toward understanding the behavior of Love modes is much more limited in the nonlinear regime,[25] and for the case of realistic, smooth vorticity profiles with finite edge gradients that are not well described by the vortex patch model.[26]

The $m = 3$ and 4 Love modes are linearly unstable for $\lambda > 3.0$ and $\lambda > 4.6$, respectively, but higher aspect ratios are required for the instability to proceed to nonlinear saturation and result in splitting. Dritschel analytically calculated an aspect ratio splitting threshold of $\lambda_s = 6.04$ based on energy conservation between the elliptical vortex patch and two-vortex equilibria.[27] Contour dynamics simulations of initially elliptical vortex patches were consistent with this result, but it was found that the splitting threshold could be reduced if the vortex was seeded with a sufficiently large amplitude $m = 4$ Love mode.[13]

Vortex patch models have been implemented in the analysis of geophysical vortex splitting events. Specifically, the Kida model for vortices subject to external shear and strain flows[28] has been applied to understand the evolution of the aspect ratio of Earth's polar vortices.[29,30] However, it rarely exceeds the $m = 3$ Love instability threshold of $\lambda = 3$ and does not come near the vortex patch splitting threshold quoted above. Furthermore, the polar vortices typically feature weak-vorticity "surf zones" at their edges due to repeated growth and breaking of Rossby waves, and so their dynamics may not be well described by the idealized vortex patch model. This motivates further investigation into the basic nonlinear physics of Love modes on vortices with smooth profiles.

Presented here are laboratory experiments and simulations of binary vortex splitting events, showing that the aspect ratio required for splitting depends strongly on the edge vorticity gradient, ranging up to twice that predicted by the vortex patch model. The experiments are carried out using collisionless, magnetized, non-neutral pure electron plasmas in a regime where the $E \times B$ drift dynamics perpendicular to the magnetic field is well described by the Drift–Poisson equations, which are isomorphic to the 2D Euler equations describing ideal fluids. Thus, the dynamics of the electron distribution accurately models that of vorticity in a 2D ideal fluid, an analogy which has been used extensively to study 2D fluids in a way not possible with traditional fluid experiments (i.e., water tanks).

Here, elliptical electron vortices are prepared using applied strain flows[31] and then allowed to evolve freely. The initial aspect ratio, λ_0, is varied in order to find the splitting threshold. An example of electron plasma data from this procedure is shown in Fig. 1 with images of the electron density or vorticity distribution obtained by accelerating the electrons onto a phosphor screen imaged by a CCD camera. In the upper row, $\lambda_0 = 7.9$ and the vortex does not split. In the lower row, $\lambda_0 = 10.7$ and the vortex splits into two approximately equal pieces. The rotating wall technique[32] is used to adjust the edge electron vorticity gradient, and the process is repeated, revealing a dependence of the splitting threshold on the profile smoothness. Interestingly, asymmetric splitting events are observed in which one of the split products contains significantly less circulation than the other. To support the experimental results, the 2D Euler equations are solved numerically using a particle-in-cell method based on point-vortex dynamics.[33] The simulation results agree closely with those of the experiments. It is observed that the vortex aspect ratio decreases over time, which modifies the Love mode growth and stability. This is thought to be due to spatial Landau damping (also known as critical-layer damping).[34–37] A simple model accounting for this effect is compared to measurements of Love mode growth in the experiments. The possible influence of the circular boundary on the splitting threshold is also discussed.

This manuscript is organized in the following way. In Sec. II, an overview of the experimental apparatus and numerical simulation technique is described, including a description of the analogy between pure electron plasmas and 2D fluids. In Sec. III, measurements of the aspect ratio threshold for vortex splitting are presented and discussed. An analysis of Love mode dynamics is given in Sec. IV. Finally, in Sec. V, a summary and conclusions are provided.

II. EXPERIMENTAL AND NUMERICAL TECHNIQUE

The isomorphism between the Drift–Poisson equations describing the $E \times B$ drift of non-neutral electron plasmas perpendicular to the magnetic field and the 2D Euler equations describing ideal fluid dynamics has been widely studied. Experiments are typically performed in a Penning–Malmberg trap, a device in which a set of hollow, cylindrical electrodes is immersed in a strong axial magnetic field in ultrahigh vacuum conditions. The magnetic field provides radial confinement of the particles, whereas electrostatic potentials applied to electrodes at either end of the trap are used to confine the particles axially. Notable examples include the discovery of vortex crystals in the laboratory,[38,39] studies of vortex merging,[40–42] and experiments on vortex oscillations and instability due to applied strain flows.[31,37,43–45]

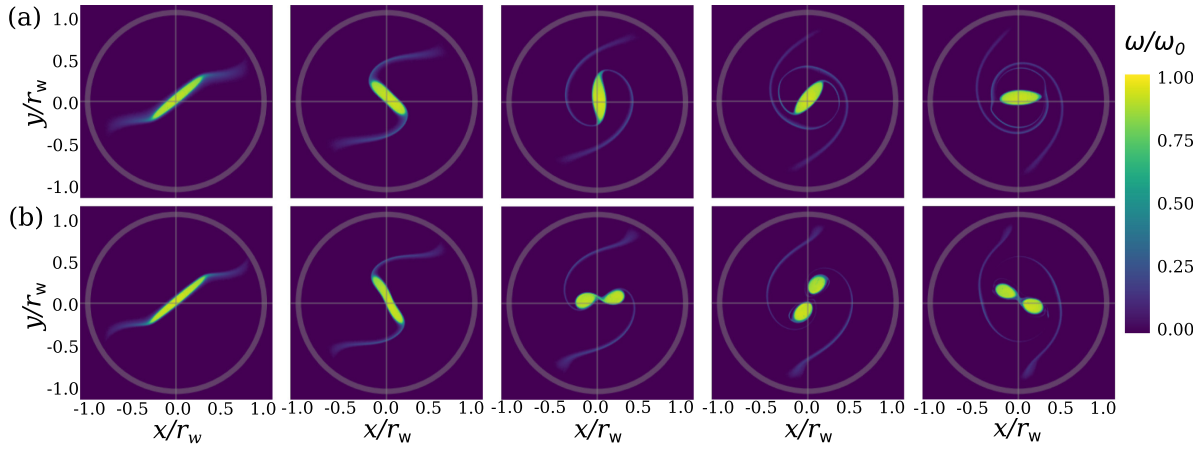

FIG. 1. The free relaxation of an elliptical vortex inside a circular boundary is shown for two cases with initial aspect ratio (a) $\lambda_0 = 7.9$ and (b) $\lambda_0 = 10.7$, using data from electron plasma experiments at normalized times $\omega_0 t$ evenly spaced from 0 to 47.2. In the latter case, the vortex splits into two pieces, whereas in the former, it does not, yielding a measurement of the aspect ratio threshold for vortex splitting.

The Drift–Poisson equations are given by

$$\left[\partial_t - \frac{1}{B}\nabla\phi \times \hat{\mathbf{z}}\cdot\nabla\right] n = 0; \quad \nabla^2\phi = en/\varepsilon_0, \tag{2}$$

where B is the magnetic field, ϕ is the electrostatic potential, n is the electron density, e is the electron charge, and ε_0 is the permittivity of free space. They are identical to Eq. (1) under the transformations $en/B\varepsilon_0 \to \omega$ and $\phi/B \to \psi$, so the electron density is analogous to the fluid vorticity, and the electric potential is analogous to the fluid stream function. Equations (2) describe the $E \times B$ drift motion of electrons due to their self-electric field as well as applied electric fields associated with boundary conditions.

The isomorphism relies on a separation of spatial and frequency scales

$$f_c \gg f_b \gg f_E \gg f_d, \tag{3}$$

where f_c is the cyclotron frequency, f_b is the axial bounce frequency between confining electrostatic potentials of the trap, f_E is the characteristic frequency of the drift motion, and f_d is the frequency scale associated with dissipation due to particle collisions. Additionally, spatial scales must follow the ordering

$$r_c \ll r_E < r_w \ll L, \tag{4}$$

where r_c is the cyclotron radius, r_E is the characteristic scale of the electron drift motion, r_w is the radius of the trap wall, and L is the axial length of the plasma. This ensures that the drift dynamics are decoupled from other plasma effects that break the analogy, including cyclotron and axial bounce motion, collisional dissipation, and 3D effects due to confining electric potentials at the trap ends.

Although the frequency and spatial scale separations given in Eqs. (3) and (4) are well-satisfied in the experiments, it is important to understand the consequences of collisional and 3D physics. Collisional dissipation in an electron plasma depends on the presence of particles and, thus, acts like a vorticity-dependent viscosity, which is inconsistent with traditional fluid viscosity in the Navier–Stokes equations. The electron fluid system features free-slip boundary conditions to a good approximation due to the lack of viscous drag between the wall and the plasma. However in practice, small asymmetries in the circular boundary place torques on the plasma and break angular momentum conservation on very long timescales. In general, 3D and finite cyclotron radius effects can cause smearing of small-scale structures and, thus, act like dissipation mechanisms.[46] The radial component of the confining electric field at ends of the trap also causes weak $E \times B$ rotation with frequency on the order of 100 Hz. These non-fluid effects are not expected to significantly impact the vortex dynamics in the experiments presented here.

The apparatus used for the experiments is called the 8-segment trap (8ST), shown schematically in Fig. 2.[47] Its key feature is a long electrode labeled *iii* in panel (a), which is segmented azimuthally into eight parts that can be biased independently. This allows for the creation of perpendicular, externally applied electric fields, which cause drift advection of the electrons without introducing strong axial electric fields that would invalidate the plasma/fluid analogy (e.g., due to axial particle trapping). This technique has been used to study vortex dynamics in applied strain flows.[31,37,43–45] The 8ST also features three short, solid electrodes *ii*, *iv*, and *vi* that are used for axial confinement of the plasma. Another short electrode labeled *v* is segmented into four pieces and used to control the electron density profile with the rotating wall (RW) technique.[32] The apparatus sits in a vacuum chamber evacuated to a pressure of about 10^{-9} Torr. Typical values of experimental parameters in the 8ST are given in Table I, where T is the plasma temperature and N is the total number of particles, showing that the separations of spatial and temporal scales given in Eqs. (3) and (4) are satisfied by at least an order of magnitude. Although viscous effects are not included in the plasma/fluid analogy, the Reynolds number in 8ST experiments is estimated to be $Re \sim 10^6$ based on decay of the peak vorticity.[43]

Experiments in the 8ST are conducted in the following way: First, a heated-cathode electron gun is used to inject electrons into the trap, where they fall into an electrostatic potential well with a depth of -100 V created between electrodes *ii* and *vi*. Then, the radial density profile is controlled using the RW electrode by applying a transverse electric field that rotates near the plasma $E \times B$ rotation frequency.

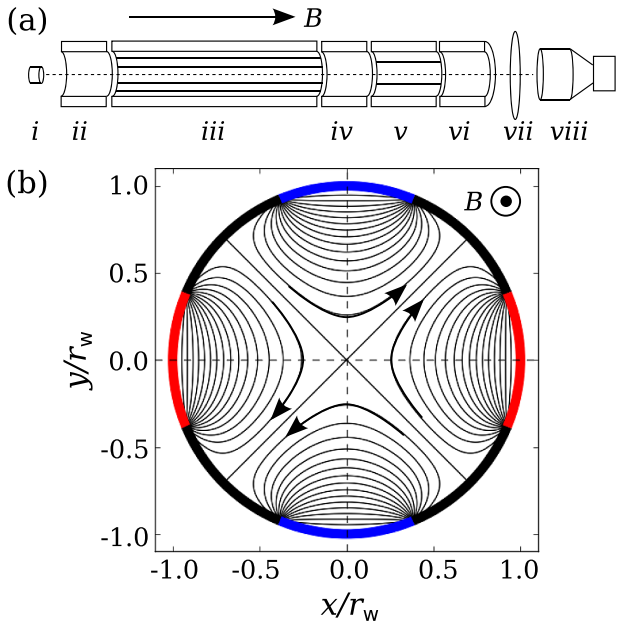

FIG. 2. Schematic of the 8ST experimental apparatus. (a) Side view of the electrode structure (*ii–vi*), with electron gun (*i*), phosphor screen (*vii*), and CCD camera (*viii*). (b) View along the magnetic field of the 8-segment electrodes biased to potential $\pm V$ (red/blue), with resulting streamlines of the applied $E \times B$ strain flow (black).

TABLE I. Typical values of experimental parameters in the 8ST.

Parameter	Value	Parameter	Value
B	4.8 T	r_c	0.5 μm
L	0.24 m	r_E	0.1–10 mm
T	$\sim$0.1 eV	f_c	130 GHz
r_w	13 mm	f_b	$\sim$1 MHz
N	$10^8 - 10^9$	f_E	10–100 kHz
n	$10^{13} - 10^{15}$ m^{-3}	f_d	$\sim$1 kHz

This results in an axisymmetric electron density (vorticity) distribution centered near the cylindrical axis of the electrodes. Examples of radial profiles prepared in this way are shown in Fig. 3, along with least squares numerical fits to the formula

$$\omega(r) = \omega_0 \exp\left[-(r/r_v)^s\right], \tag{5}$$

where ω_0 is the peak vorticity, r_v is the vortex radius, and s is a parameter characterizing the profile smoothness or edge gradient. The vortex patch distribution (i.e., the Rankine vortex) corresponds to $s \to \infty$, and $s = 2$ is a Gaussian profile. The blue profile in Fig. 3 with $\omega_0 = 580$ krad/s is used for all data presented here, unless otherwise specified.

Following this, the RW electrode is grounded, and one segment of electrode *iii* is connected to a feedback circuit that damps the $m = 1$ diocotron mode, placing the plasma density centroid very close to the axis. The damping circuit is then turned off, electrode *iv* is ramped to -100 V, and the remaining plasma confined between electrodes *iv* and

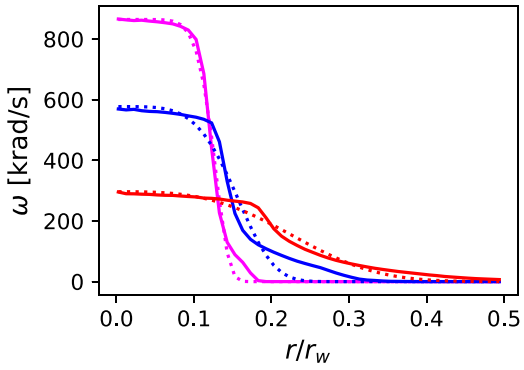

FIG. 3. Initial axisymmetric vorticity profiles measured in the experiment, along with least-square fits to Eq. (5) (dotted), yielding $s = 8.6$ (magenta), 4.5 (blue), and 3.1 (red).

vi is discarded by ramping electrode *vi* to ground. At this point, an electron plasma with the desired radial density profile is confined under electrode *iii*. This electrode is then used to apply an external $E \times B$ flow to study vortex dynamics within the bounds of the plasma/fluid analogy. Sometime later, electrode *iv* is ramped quickly to ground such that the trapped plasma travels axially along the field, where it is accelerated onto a phosphor screen biased to $+5$ kV. The resulting light is diagnosed with a CCD camera with a resolution of 31 pixels/mm and signal-to-noise ratio on the order of 100. This yields a destructive measurement of the 2D electron density or vorticity distribution at one point in time, integrated along the axial direction.

Vortex splitting experiments are conducted by preparing elliptical vortices using strong external strain flows and then turning off the strain such that the electron fluid is allowed to relax freely inside the circular boundary. Strain flows are created by applying quadrupolar potentials to the eight-segment electrode, as shown in Fig. 2(b). The eight segments are biased to voltages $[+V, 0, -V, 0, +V, 0, -V, 0]$, beginning on the x axis. Near the origin at the axis of the trap, this results in an $E \times B$ flow described by

$$\psi = \frac{1}{2}\varepsilon(x^2 - y^2); \ \mathbf{v} = \varepsilon(y\hat{\mathbf{x}} - x\hat{\mathbf{y}}), \tag{6}$$

where $\varepsilon = 1.8V/Br_w^2$ is the strain rate. If the strain-to-vorticity ratio ε/ω is sufficiently large, the self-generated flow due to the vorticity is relatively weak and so the vorticity approximately experiences passive advection. This causes an initially circular vortex to deform elliptically with aspect ratio $\lambda(t) = \exp(2\varepsilon\Delta t)$, where Δt is the duration of the applied strain flow. In this way, elliptical vortices with specific aspect ratios can be prepared.

To study the vortex evolution, the sampling time was varied over a series of experimental runs. Three runs are taken at each time in order to measure the experimental uncertainty, which is typically set by the initial filling of the trap with plasma with density variations $\delta n/n$ of a few percent from run to run. To assess whether vortex splitting has occurred without regard to details of the evolution, one particular sampling time is chosen, which is long compared to the instability and saturation time ($\omega_0 t \sim 50$).

Numerical simulations are conducted by solving the 2D Euler equations approximately using a particle-in-cell method. The particles represent point vortices that obey the Hamiltonian

$$H = \Gamma \sum_{i=i}^{N} \psi_{\text{ext}}(\mathbf{r_i}) + \Gamma^2 \sum_{i \neq j} G(\mathbf{r_i}, \mathbf{r_j}), \tag{7}$$

where ψ_{ext} is the applied flow due to the boundary conditions, G is the Green's function for the 2D Poisson equation, and $\mathbf{r_i}$ is the location of the point vortices. The point vortices are initially arranged using a Monte Carlo method to approximate a smooth, elliptical vorticity distribution with aspect ratio λ, which is defined by Eq. (5) with spatial coordinates rescaled as $(x, y) \rightarrow \left(x/\sqrt{\lambda}\right), \left(y\sqrt{\lambda}\right)$. The stream function is calculated on a rectangular grid using a sparse matrix solver. It is used to advance the vortices with a fourth-order Runge–Kutta algorithm. The boundary condition is set by imposing constant stream function on the circular wall, as represented on the rectangular grid. The simulations are conducted on a grid of 500^2 elements with 10^6 point vortices.

III. VORTEX SPLITTING THRESHOLD MEASUREMENTS

Vortex splitting events can be identified by topological changes in the stream function and vorticity fields. The topology of the stream function before and after splitting in the frame rotating with the vortex (or vortices) is shown in Fig. 4. The Poisson equation is solved numerically to determine ψ from the vorticity measurement. The rotation rate Ω is determined, and ψ is boosted into the rotating frame by adding a uniform background vorticity term $\frac{1}{2}\Omega r^2$. For the initially elliptical vortex, there exists an O-point (center point) at the vortex core, two X-points (saddle points) along the major axis near the tips of the vortex and two O-points along the minor axis. When the vortex splits, the central O-point bifurcates into an O-X-O configuration, where the two O-points are centered on the split products and the X-point defines a separatrix enclosing them.

In a 2D ideal fluid described by Eq. (1), the vorticity field cannot change topology since it is conserved in the Lagrangian frame. However, after a splitting event, the two products are connected by a filament of vorticity, which rapidly thins and is, therefore, subject to coarse-graining due to the diagnostic resolution in the experiment or finite-particle effects in the simulations. This causes the measured vorticity in the filament to decrease and, thus, changes the topology of the vorticity field. This way, late-time vorticity measurements can be used to evaluate whether splitting has occurred. In addition, the ratio of circulations contained in the two split products, $\Gamma_1/\Gamma_2 \in [0, 1]$, can be estimated by measuring the average radii of the half-maximum vorticity contours $\langle r_v \rangle$, where $\Gamma_1/\Gamma_2 = (\langle r_{v1} \rangle / \langle r_{v2} \rangle)^2$.

Since the Love mode growth on an elliptical vortex patch depends only on the aspect ratio λ, we use this as a control parameter to study the vortex splitting bifurcation. Different initial vorticity profiles with varying levels of peak vorticity, vortex radius, and smoothness (or edge gradient) are prepared, as shown in Fig. 3. The axisymmetric vortices are stretched to initial aspect ratios λ_0 using applied strain flows as described in Sec. II and then allowed to relax freely. The initial aspect ratio is increased over subsequent experimental runs until splitting is observed, yielding measurements of the aspect ratio splitting threshold, λ_s.

A few important qualitative observations of the vortex splitting process were made. First, in all of the experiments and simulations presented here, once a vortex had split into two pieces, the new configuration was metastable, meaning that they did not re-merge over many rotations, although this would eventually happen on a dissipative timescale due to diffusive growth of $\langle r_v \rangle$. Second, in many cases, the split products were born with oscillatory surface perturbations (e.g., Kelvin modes), so that the post-splitting vorticity distribution was non-steady in the rotating frame. Third, in some cases, near the threshold, asymmetric splitting was observed in which $\Gamma_1/\Gamma_2 \ll 1$, as shown in Fig. 5. This is likely due to the growth of an $m = 3$ Love mode, as opposed to (or in addition to) the $m = 4$ mode implicated in symmetric splitting events. This phenomenon was observed recently in PIC simulations but not studied in detail.[48] Finally, binary splitting events were not observed for nearly Gaussian vorticity profiles with $s \lesssim 3$. Rather, the strong vortex core remained intact, while two filamentary arms generated by the strain flow collapsed into two small satellite vortices.

The theoretical vortex patch analysis from Dritschel did not account for asymmetric splitting.[27] These events are associated with topological changes and can be classified as vortex splitting bifurcations, although Γ_1/Γ_2 does not change abruptly from 0 to 1 as λ_0 is varied. For this reason, we define λ_s as a range, where the lower bound corresponds to the largest λ_0 tested for which the system does not bifurcate, and the upper bound corresponds to the smallest λ_0 for

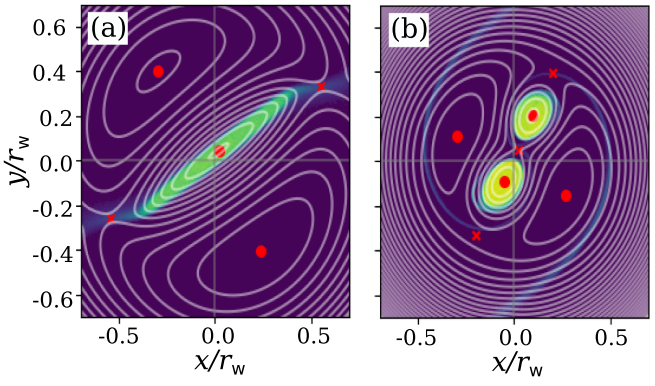

FIG. 4. The vorticity (colormap) and stream function in the rotating frame (white contours) are shown for $\lambda_0 = 10.7$ at times $\omega_0 t = 0$ (left) and 35.4 (right). Center and saddle fixed-points of the stream function are marked with red circles and crosses, respectively, indicating a topological change associated with vortex splitting.

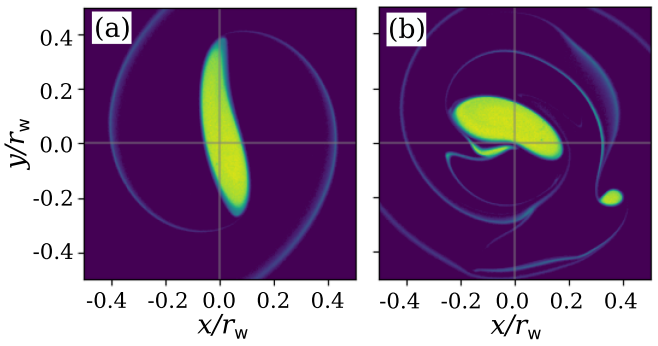

FIG. 5. Vorticity data are shown at normalized times $\omega_0 t =$ (a) 29.5 and (b) 76.7 with initial aspect ratio $\lambda_0 = 9.1$, resulting in the growth of an $m = 3$ Love mode shown in panel (a) and an asymmetric splitting event with $\Gamma_1/\Gamma_2 \sim 0.1$ shown in panel (b).

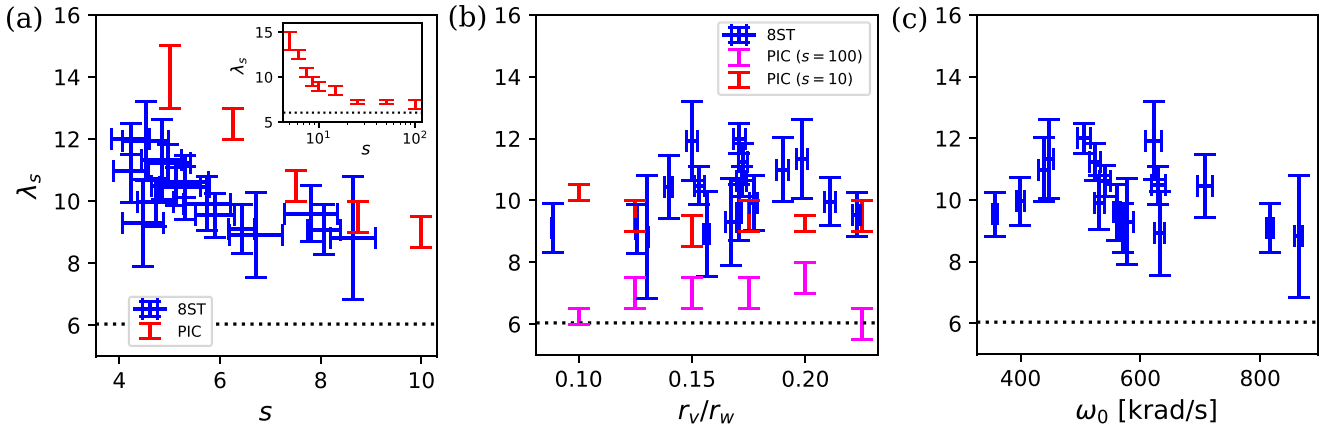

FIG. 6. The aspect ratio splitting threshold λ_s is plotted vs (a) the vortex smoothness parameter, (b) the normalized vortex radius, and (c) the peak vorticity, for experimental measurements using electron plasmas in the 8ST and PIC simulations. The theoretical prediction from Dritschel[27] is shown as a dotted line. In panel (a), the simulations use $r_v/r_w = 0.15$, and the inset shows simulation data for $5 \leq s \leq 100$. In panel (b), two values of s are shown, where $s = 100$ closely approximates the vortex patch distribution.

which splitting is observed with $\Gamma_1/\Gamma_2 \geq 1/2$ (a somewhat arbitrary choice based on the distribution of circulation ratios observed in the experiments and simulations).

Analytical profiles given by Eq. (5) were numerically fitted to a set of 17 experimentally measured axisymmetric vorticity profiles in order to extract values of s, r_v, and ω_0 for each case. In Fig. 6, the measured binary split threshold λ_s is plotted against each fit parameter for all profiles tested in the experiments. Also plotted are threshold measurements from numerical PIC simulations with profiles given by Eq. (5), and the vortex patch analytical prediction $\lambda_s = 6.04$. The large error bars reflect uncertainty in the experimental and numerical results, the prevalence of asymmetric splitting events, and the resolution of the λ_0 scan performed.

An important observation is that all of the experimental vortices tested show splitting thresholds well above the vortex patch prediction. Furthermore, a clear dependence on the vortex smoothness parameter s is observed in both the experiments and simulations. Due to limitations on the vorticity profile control technique, the experimental vortices are limited to roughly $s < 10$. The simulation data show that λ_s tends toward the theoretical prediction as s increases but reaches a minimum of about 7 for $s \geq 25$. Boundary effects are expected to impact the splitting threshold at some value of the normalized vortex radius r_v/r_w. In particular, the non-axisymmetric vorticity distribution induces image vorticity at $r/r_w > 1$, which causes adverse rotation near the tips of the vortex. In the most extreme case of Fig. 6(b), the tips of an elliptical vortex patch with $r_v/r_w = 0.225$ and $\lambda = 12$ extend to $r/r_w = 0.78$ along the major axis. Interestingly, no strong dependence of the splitting threshold on r_v/r_w is observed in the experiments. Simulations with $s = 10$ and $s = 100$ are shown in Fig. 6(b), where the former is representative of the experiments, and the latter corresponds closely to the vortex patch model. The small variations in λ_s with r_v from the simulations and the slight discrepancy between the simulations with large s and the theoretical vortex patch prediction may be due to boundary effects, but more work is needed to clarify this.

Varying ω_0 simply rescales time in Eq. (1) and otherwise has no impact on the fluid dynamics. Thus, any dependence of the experimental splitting threshold on ω_0 would indicate non-fluid effects. For example, at high vorticity, the vortex rotation rate approaches the axial bounce frequency of the electrons, introducing 3D physics. No significant dependence on ω_0 is observed within the uncertainty of the measurements, so any such non-fluid effects present in the experiment appear to have little effect on the splitting threshold.

Notably, λ_s from the simulations exceeds that from the experiments in Fig. 6(a) for $s \leq 7$. This is likely due to discrepancies between the vorticity profiles measured in the experiments and Eq. (5) used for the simulations. In particular, the experimental vortices tend to have higher vorticity gradients near $r = r_v$ and weaker gradients at larger r (see Fig. 3). Further simulations were conducted to more accurately model the experimental procedure. The initial axisymmetric vorticity profile measured in the experiment was reproduced in the simulations and stretched into an elliptical shape using an applied strain flow. For simulations corresponding to the data shown in Fig. 1, this yielded $\lambda_s = (8.9, 10.6)$, which is consistent with the experimental result of $\lambda_s = (7.9, 10.7)$, giving confidence that the electron plasma experiments are a faithful representation of 2D fluid dynamics.

IV. LOVE MODE ANALYSIS

Love modes are linearized perturbations of the edge of an elliptical vortex patch.[24] They describe the linear stability of the Kirchoff rotating vortex solution to the 2D Euler equations.[22,23] A modern analytical treatment of the Love instability is given by Guo *et al.*[25] The analysis is conducted in an elliptical coordinate system (μ, ν), which is related to the Cartesian coordinates by

$$x = c \cosh\mu \cos\nu; \quad y = c \sinh\mu \sin\nu. \tag{8}$$

The unperturbed vortex edge is given by $\mu = \mu_0 = \tanh^{-1}(b/a)$, and the focus is given by $c^2 = a^2 - b^2$. Displacements of the vortex edge are described by

$$q(\nu) = J_0(\nu)\delta\mu(\nu) = \sum_{m=1}^{\infty} \alpha_m \cos[m(\nu - \beta_m)], \tag{9}$$

where $\delta\mu = \mu - \mu_0$ is the displacement in elliptical coordinates, $J_0(\mu) = a^2 \sin^2\nu + b^2 \cos^2\nu$ is the Jacobian used to change between

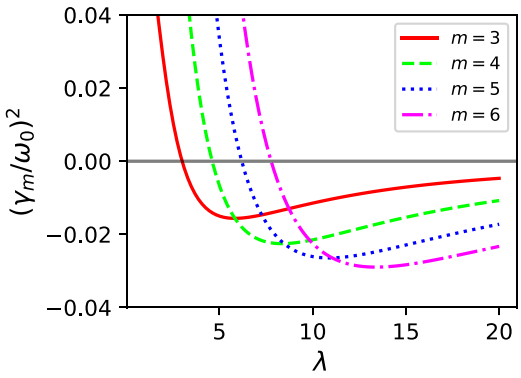

FIG. 7. Love mode growth rate for various m, where negative and positive $(\gamma_m/\omega_0)^2$ indicate instability and stable rotation, respectively.

Cartesian and elliptical coordinates, α_m and β_m are the mode amplitude and phase, respectively, and m is the wavenumber. These modes evolve in time as $\exp(-i\gamma_m t)$, where the normalized growth rate

$$\left(\frac{\gamma_m}{\omega_0}\right)^2 = \frac{1}{4}\left[\left[\frac{2m\lambda}{(\lambda+1)^2}-1\right]^2-\left(\frac{\lambda-1}{\lambda+1}\right)^{2m}\right] \tag{10}$$

depends only on the aspect ratio λ of the unperturbed vortex for a particular m. It is shown in Fig. 7 for $3 \leq m \leq 6$. Wavenumbers $m=1$ and 2 correspond to translation and elliptical deformation of the vortex, respectively, and they are never unstable. For each mode with $m \geq 3$, there exists a critical value λ_c above which the modes are unstable and below which they exhibit stable rotation. This critical value increases with m, and the wavenumber of the fastest growing mode increases with λ. For $m=3$ and 4, $\lambda_c = 3$ and 4.6, respectively. In the limit $\lambda \to \infty$, on the scale of the fastest growing mode, the local vorticity distribution can be approximated as a rectangular shear layer, and so the Love instability is equivalent to the Kelvin–Helmholtz instability. In the limit $\lambda \to 1$, the Love modes are equivalent to Kelvin modes propagating on a circular (Rankine) vortex. The shape of the unstable eigenmode for $m=3$ features an elongated tip on one side of the vortex along the major axis [see Fig. 5(a)], which can develop into an asymmetric splitting event as discussed in Sec. III.[13] The unstable eigenmode for $m=4$ has the shape of a peanut, with two lobes along the major axis that develop into independent vortices during a splitting event.

Love mode properties of the electron plasma vortices are extracted from experimental measurements of the vorticity distribution, as shown in Fig. 8. In panel (a), the half-maximum vorticity contour is found by identifying pixels with $0.4 < \omega/\omega_0 < 0.6$. An ellipse is numerically fitted to these points using a least squares algorithm to extract values of a and b, and the ellipse orientation ξ. The data are rotated about their centroid by the angle ξ so that the major axis of the ellipse lies along the x axis, and plotted in panel (b) along with the fitted ellipse and the elliptical coordinate grid that it defines. The data are transformed to elliptical coordinates (μ, ν), and the displacement $q(\nu)$ is plotted in panel (c), along with a smooth spline, which is fitted to the data in order to reduce experimental noise. Finally, the Love mode amplitudes are calculated by taking the Fast Fourier Transform (FFT) of the spline in panel (c), and the results are shown in panel (d). The example shown in Fig. 8 corresponds to the second panel in Fig. 1(b). A strong $m=4$ Love mode is detected, which develops into a near-symmetric splitting event later in time.

For the highly elliptical vortices considered here, the Love mode fitting routine fails at some time during the vortex evolution for several reasons. For sufficiently large mode amplitudes and particular phases, the half-maximum vorticity contour intersects the semimajor axis at a location(s) $|x| < c$, and so the curve becomes discontinuous in the angular elliptical coordinate near $\nu = 0$ and $\pm\pi$ [see Fig. 8(c)]. In this case, Love's theory based on elliptical coordinates becomes ill-posed. The fitting routine can still be carried out, but its accuracy decreases with the width of the discontinuity. During vortex splitting events, the half-maximum contour becomes highly distorted, and the fitting routine becomes unreliable, in part due to the difficulty in fitting the unperturbed ellipse. In cases that do not split, the routine can fail instead due to filamentation at the tips of the vortex, which can be seen in the third panel of Fig. 1(a).

The fitted values of λ and the Love mode amplitudes α_3 and α_4 are shown in Fig. 9 for $\lambda_0 = 7.9$, 9.1, and 10.7. Over three repetitions of the experiment, the first case did not split, the second split asymmetrically in some instances, and the third split with near-symmetry in all instances. Importantly, panel (a) shows that the aspect ratio of the fitted ellipse decreases over time in all cases. Early in time, the decay is

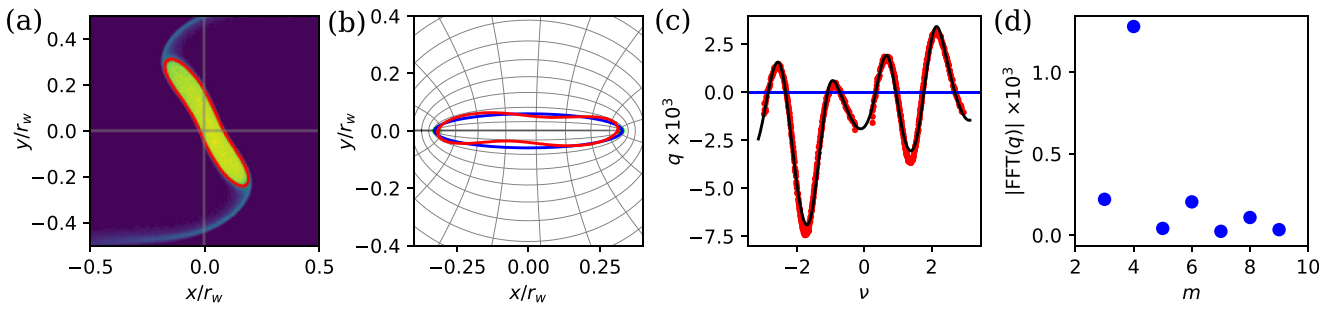

FIG. 8. An example of the Love mode fitting routine used for electron plasma vortices in the 8ST. (a) The half-maximum vorticity contour (red) is plotted over vorticity data (colormap); (b) the contour (red) is plotted along with the fitted ellipse (blue) and corresponding elliptical coordinate grid (black); (c) the displacement of the vortex edge is plotted vs the angular elliptical coordinate ν (red) along with a smooth spline fit (black); and (d) the FFT of the curve in (c) quantifies the amplitude of Love modes with wavenumber m. The example shown has $\lambda_0 = 10.7$ and $\omega_0 t = 17.7$, with a strong $m=4$ mode.

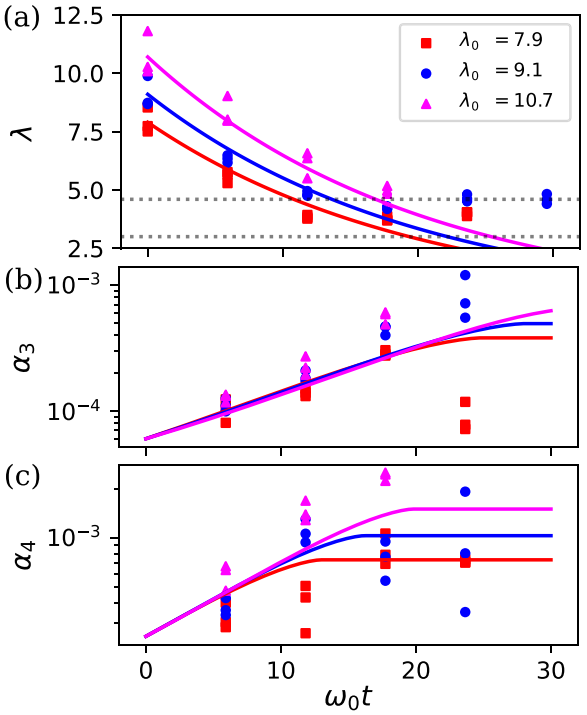

FIG. 9. Love mode amplitude evolution extracted from vorticity data, including (a) the unperturbed ellipse aspect ratio, and (b) and (c) the $m = 3$ and 4 Love mode amplitudes, respectively. Three cases are shown with $\lambda_0 = 7.9$ (red squares), 9.1 (blue circles), and 10.7 (magenta triangles). In panel (a), the stability thresholds λ_c are indicated for the $m = 3$ and 4 Love modes (dotted lines), and exponential functions (solid lines) are fitted to the data as described in the text. In panels (b) and (c), a simple model is shown (solid lines) in which the Love mode growth rate and stability vary in time.

well described by an exponential function $\lambda(t) = \lambda_0 \exp(-t/\tau)$ with a normalized time constant $\omega_0\tau = 20$, which is plotted over the data. This changes the linear growth rate and stability of the Love modes over time. In particular, the $m = 4$ mode implicated in vortex splitting is stabilized earlier for smaller λ_0.

The aspect ratio or quadrupole moment of an initially elliptical vortex can decay through a mechanism known as inviscid spatial Landau damping in the context of pure electron plasmas,[34,35,37] or critical-layer damping in fluid dynamics.[36,49] Here, the damping occurs due to fluid motion in the two spatial dimensions, in analogy with velocity-space Landau damping in kinetic plasma systems. It is due to the resonant interaction of the rotating fluid with the rotating elliptical mode at a particular radius known as the critical layer, where the damping rate is proportional to the vorticity gradient at this location. In the linear stage, filaments form at the tips of the elliptical vortex, and the nonlinear stage is marked by the trapping of fluid in "islands" or stable regions on either side of the vortex along the minor axis. The vortex evolution observed here is qualitatively consistent with this mechanism, although damping has not been studied extensively for such large aspect ratios.

Using the exponential decay curves for $\lambda(t)$ described in the context of Fig. 9(a), the evolution of α_3 and α_4 is modeled and plotted over the data in panels (b) and (c). In the model, the mode amplitude grows

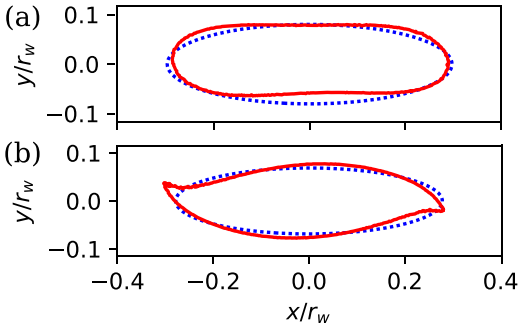

FIG. 10. The half-maximum vorticity contour (red) and unperturbed ellipse (blue, dotted) are shown for $\lambda_0 = 7.9$ at times $\omega_0 t =$ (a) 17.7 and (b) 23.6.

according to Eq. (10) and stops growing when $\lambda < \lambda_c$. The data show approximately exponential growth early in time, but the amplitude levels off later in time for lower values of λ_0. Mode amplitudes could not be reliably obtained from the data at $t = 0$ due to low signal-to-noise ratio, so the initial amplitude in the model was chosen to roughly match the data later in time. Data are not shown at late times where the fitting routine breaks down. The case with $\lambda_0 = 9.1$ that produced asymmetric splitting events yields large values of α_3. The case with $\lambda_0 = 10.7$ that produced near-symmetric splitting events yields large values of α_4. Thus, the simple model predicts larger-amplitude modes for higher λ_0 simply because the mode has more time to grow before becoming stable due to decay of the aspect ratio. Discrepancies between the data and the simple model may be due to the unknown initial amplitude and phase; nonlinear effects that could modify growth and/or exchange energy between modes at large amplitude; and the direct influence of profile smoothness on the Love mode dynamics.

When $\lambda < \lambda_c$, the Love modes are expected to rotate. Figure 10 shows the half-maximum contours for the case with $\lambda_0 = 7.9$ below the splitting threshold at times $\omega_0 t =$ (a) 17.7 and (b) 23.6. In panel (a), an $m = 4$ mode is clearly visible with phase near $\pi/4$ (peanut shape), and in panel (b), the phase is near 0 (eye shape), indicating that the mode has rotated due to the decreasing aspect ratio.

V. SUMMARY AND CONCLUSIONS

The results presented here show that the aspect ratio threshold for binary vortex splitting, λ_s, ranges from 8 to 12 for vortices with realistic, smooth vorticity profiles, significantly higher than the analytical prediction of $\lambda_s = 6.04$ for the idealized vortex patch model in which the edge vorticity gradient is infinite.[27] This conclusion is borne out in non-neutral electron plasma experiments for which the $E \times B$ drift dynamics is analogous to those of a 2D ideal fluid, and in particle-in-cell simulations that solve for the motion of a set of point vortices. While the circular boundary is expected to impact the vortex splitting process at some level, the weak variation of the splitting threshold with vortex radius indicates that boundary effects are relatively unimportant in this work. Agreement between the experiments and simulations, and independence of the experimental results on the electron density give confidence that the experiments are a faithful representation of 2D ideal fluid dynamics.

Analysis of the vortex evolution reveals that the aspect ratio of an ellipse fitted to the vorticity distribution decreases significantly over time. This is presumably due to a spatial Landau (or critical-layer)

damping mechanism similar to that studied previously at lower aspect ratio.[35,36] As a result, the Love mode growth and stability properties change over time, such that the $m = 3$ and 4 modes stop growing at some point and begin to rotate. Thus, in order to grow to large enough amplitude to proceed to nonlinear saturation and cause the vortex to split, the initial aspect ratio must be large. In comparison, the vortex patch model does not exhibit Landau damping due to the lack of vorticity gradient at the resonant layer, and so splitting can occur for smaller initial aspect ratio. It is possible that the Love mode dynamics are also modified directly by the smooth vorticity profile and/or by nonlinear mode interactions, but these topics are left for future work.

Another important finding is that near the splitting threshold, the growth of $m = 3$ Love modes can lead to asymmetric splitting events. Thus, the onset of vortex splitting with increasing aspect ratio is gradual rather than sudden, with the circulation ratio of the resulting two vortices varying smoothly from zero to unity. However, events with circulation ratio near zero may be of less practical importance than those near unity, since relatively little fluid is contained in the smaller split product.

These results may be relevant to atmospheric vortex splitting events at the poles of Earth and other planets. Usage of the vortex patch model in the analysis of these events[29,30] may be complicated by the effect of Landau damping, for example, due to the edge vorticity gradient associated with the Rossby-wave surf zone. Additionally, the role of the symmetry-breaking $m = 3$ Love mode in setting the circulation ratio should be considered. The aspect ratios of Earth's polar vortices do not typically approach the vortex patch splitting threshold of $\lambda_s = 6.04$ and are far from the thresholds measured here for smooth vortices. Thus, they are unlikely to split due to the free growth of Love modes, so forcing is probably necessary (e.g., due to topography and/or the influence of other vortices at lower latitudes). For drift-wave eddies in fusion plasmas,[19] these results indicate that splitting may be more unlikely than previously thought due to the relatively high aspect ratios required.

ACKNOWLEDGMENTS

This work was supported by the U.S. Department of Energy (DOE) under Grant Nos. DE-SC0016532 and DE-SC0018236; the Wisconsin Plasma Physics Laboratory (WiPPL), a research facility supported by the DOE under Contract No. DE-SC0018266; the U.S. National Science Foundation under Grant No. PHY 2106332, and the Office of the Permanent Secretary, Ministry of Higher Education, Science, Research and Innovation (Thailand) under Grant No. RGNS 65-106.

AUTHOR DECLARATIONS

Conflict of Interest

The authors have no conflicts to disclose.

Author Contributions

N. C. Hurst: Conceptualization (lead); Formal analysis (lead); Investigation (lead); Methodology (lead); Software (lead); Visualization (lead); Writing – original draft (lead); Writing – review & editing (equal). **A. Tran:** Investigation (supporting); Methodology (supporting); Software (supporting). **P. Wongwaitayakornkul:** Conceptualization (supporting); Investigation (supporting). **J. R. Danielson:** Conceptualization (supporting); Formal analysis (supporting); Investigation (supporting); Methodology (supporting); Resources (equal); Supervision (equal); Writing – review & editing (supporting). **D. H. E. Dubin:** Conceptualization (supporting); Investigation (supporting); Supervision (equal). **C. M. Surko:** Conceptualization (supporting); Funding acquisition (lead); Project administration (lead); Supervision (equal); Writing – review & editing (supporting).

DATA AVAILABILITY

The data that support the findings of this study are available from the corresponding author upon reasonable request.

REFERENCES

[1]R. Salmon, *Lectures on Geophysical Fluid Dynamics* (Oxford University Press, New York, 1998).
[2]T. Meuel, Y. L. Xiong, P. Fischer, C. H. Bruneau, M. Bessafi, and H. Kellay, "Intensity of vortices: from soap bubbles to hurricanes," Nat. Sci. Rep. **3**, 3455 (2013).
[3]R. V. E. Lovelace, H. Li, S. A. Colgate, and A. F. Nelson, "Rossby wave instability of Keplerian accretion disks," Astrophys. J. **513**, 805 (1999).
[4]A. Adams, P. M. Chesler, and H. Liu, "Holographic turbulence," Phys. Rev. Lett. **112**, 151602 (2014).
[5]A. Hasegawa and K. Mima, "Pseudo-three-dimensional turbulence in magnetized nonuniform plasma," Phys. Fluids **21**, 87 (1978).
[6]R. H. Levy, "Diocotron instability in a cylindrical geometry," Phys. Fluids **8**, 1288 (1965).
[7]C. F. Driscoll and K. S. Fine, "Experiments on vortex dynamics in pure electron plasmas," Phys. Fluids B **2**, 1359 (1990).
[8]R. C. Davidson, *Physics of Nonneutral Plasmas* (Addison-Wesley, Redwood City, CA, 1990).
[9]D. Montgomery and L. Turner, "Two-dimensional electrostatic turbulence with variable density and pressure," Phys. Fluids **23**, 264 (1980).
[10]R. H. Kraichnan, "Inertial ranges in two-dimensional turbulence," Phys. Fluids **10**, 1417 (1967).
[11]J. P. Christiansen and N. J. Zabusky, "Instability, coalescence and fission of finite-area vortex structures," J. Fluid Mech. **61**, 219 (1973).
[12]P. Freymuth, W. Bank, and M. Palmer, "First experimental evidence of vortex splitting," Phys. Fluids **27**, 1045 (1984).
[13]T. B. Mitchell and L. F. Rossi, "The evolution of Kirchoff elliptic vortices," Phys. Fluids **20**, 54103 (2008).
[14]A. H. Butler, Z. D. Lawrence, S. H. Lee, S. P. Lillo, and C. S. Long, "Differences between the 2018 and 2019 stratospheric polar vortex split events," Quart. J. R. Meteorol. Soc. **146**, 3503 (2020).
[15]D. M. Mitchell, A. J. Charlton Perez, L. J. Gray, H. Akiyoshi, N. Butchart, S. C. Hardiman, O. Morgenstern, T. Nakamura, E. Rozanov, K. Shibata, D. Smale, and Y. Yamashita, "The nature of Arctic polar vortices in chemistry-climate models," Quart. J. R. Meteorol. Soc. **138**, 1681 (2012).
[16]A. J. Charlton, A. O'Neill, W. A. Lahoz, and P. Berrisford, "The splitting of the stratospheric polar vortex in the southern hemisphere, September 2002: Dynamical evolution," J. Atmos. Sci. **62**, 590–602 (2005).
[17]D. M. Mitchell, R. K. Scott, W. J. M. Seviour, S. I. Thomson, D. W. Waugh, N. A. Teanby, and E. R. Ball, "Polar vortices in planetary atmospheres," Rev. Geophys. **59**, e2020RG000723, https://doi.org/10.1029/2020RG000723 (2021).
[18]P. H. Diamond, S.-I. Itoh, K. Itoh, and T. S. Hahm, "Zonal flows in plasma—A review," Plasma Phys. Controlled Fusion **47**, R35 (2005).
[19]P. Manz, M. Ramisch, and U. Stroth, "Physical mechanism behind zonal-flow generation in drift-wave turbulence," Phys. Rev. Lett. **103**, 165004 (2009).
[20]N. G. Berloff, "Vortex splitting in subcritical nonlinear Schrödinger equations," Fluid Dyn. Res. **41**, 051403 (2009).
[21]Y. Shin, M. Saba, M. Vengalattore, T. A. Pasquini, C. Sanner, A. E. Leanhardt, M. Prentiss, D. E. Pritchard, and W. Ketterle, "Dynamical instability of a doubly quantized vortex in a Bose-Einstein condensate," Phys. Rev. Lett. **93**, 160406 (2004).

[22]G. Kirchhoff, *Vorlesungen Über Mathematische Physik: Mechanik* (Teubner, Leipzig, 1876).
[23]H. Lamb, *Hydrodynamics* (Cambridge University Press, 1932).
[24]A. E. H. Love, "On the stability of certain vortex motions," Proc. London Math. Soc. **s1-25**, 18 (1893).
[25]Y. Guo, C. Hallstrom, and D. Spirn, "Dynamics near an unstable Kirchhoff ellipse," Commun. Math. Phys. **245**, 297 (2004).
[26]L. Xu and R. Krasny, "Dynamics of elliptical vortices with continuous profiles," Phys. Rev. Fluids **8**, 024702 (2023).
[27]D. G. Dritschel, "The nonlinear evolution of rotating configurations of uniform vorticity," J. Fluid Mech. **172**, 157 (1986).
[28]S. Kida, "Motion of an elliptic vortex in a uniform shear flow," J. Phys. Soc. Jpn. **50**, 3517 (1981).
[29]N. J. Matthewman and J. G. Esler, "Stratospheric sudden warmings as self-tuning resonances. Part I: Vortex splitting events," J. Atmos. Sci. **68**, 2481 (2011).
[30]M. Mester and J. G. Esler, "Dynamical elliptical diagnostics of the Antarctic polar vortex," J. Atmos. Sci. **77**, 1167 (2019).
[31]N. C. Hurst, J. R. Danielson, D. H. E. Dubin, and C. M. Surko, "Evolution of a vortex in a strain flow," Phys. Rev. Lett. **117**, 235001 (2016).
[32]J. R. Danielson, C. M. Surko, and T. M. O'Neil, "High-density fixed point for radially compressed single-component plasmas," Phys. Rev. Lett. **99**, 135005 (2007).
[33]J. Goodman, T. Y. Hou, and J. Lowengrub, "Convergence of the point vortex method for the 2-D Euler equations," in *Communications on Pure and Applied Mathematics* (John Wiley and Sons, Inc., 1990), Vol. 43, p. 415.
[34]R. J. Briggs, J. D. Daugherty, and R. H. Levy, "Role of Landau damping in crossed-field electron beams and inviscid shear flow," Phys. Fluids **13**, 421 (1970).
[35]D. A. Schecter, D. H. E. Dubin, A. C. Cass, C. F. Driscoll, I. M. Lansky, and T. M. O'Neil, "Inviscid damping of asymmetries on a two-dimensional vortex," Phys. Fluids **12**, 2397 (2000).
[36]S. L. Dizes, "Non-axisymmetric vortices in two-dimensional flows," J. Fluid Mech. **406**, 175 (2000).
[37]P. Wongwaitayakornkul, J. R. Danielson, N. C. Hurst, D. H. E. Dubin, and C. M. Surko, "Inviscid damping of an elliptical vortex subject to an external strain flow," Phys. Plasmas **29**, 052107 (2022).
[38]K. S. Fine, A. C. Cass, W. G. Flynn, and C. F. Driscoll, "Relaxation of 2D turbulence to vortex crystals," Phys. Rev. Lett. **75**, 3277 (1995).
[39]A. Sanpei, Y. Kiwamoto, K. Ito, and Y. Soga, "Formation of a vortex crystal cell assisted by a background vorticity distribution," Phys. Rev. E **68**, 016404 (2003).
[40]T. B. Mitchell and C. F. Driscoll, "Electron vortex orbits and merger," Phys. Fluids **8**, 1828 (1996).
[41]M. Amoretti, D. Durkin, J. Fajans, R. Pozzoli, and M. Rome, "Asymmetric vortex merger: Experiments and simulations," Phys. Plasmas **8**, 3865 (2001).
[42]Y. Soga, Y. Kiwamoto, A. Sanpei, and J. Aoki, "Merger and binary structure formation of two discrete vortices in a background vorticity distribution of a pure electron plasma," Phys. Plasmas **10**, 3922 (2003).
[43]N. C. Hurst, J. R. Danielson, D. H. E. Dubin, and C. M. Surko, "Experimental study of the stability and dynamics of a two-dimensional ideal vortex under external strain," J. Fluid Mech. **848**, 256–287 (2018).
[44]N. C. Hurst, J. R. Danielson, D. H. E. Dubin, and C. M. Surko, "Instability of an electron-plasma shear layer in an externally imposed strain flow," Phys. Plasmas **27**, 042101 (2020).
[45]N. C. Hurst, J. R. Danielson, D. H. E. Dubin, and C. M. Surko, "Adiabatic behavior of an elliptical vortex in a time-dependent external strain flow," Phys. Rev. Fluids **6**, 054703 (2021).
[46]A. J. Peurrung and J. Fajans, "A limitation to the analogy between pure electron plasmas and two-dimensional inviscid fluids," Phys. Fluids B **5**, 4295 (1993).
[47]N. C. Hurst, J. R. Danielson, and C. M. Surko, "An electron plasma experiment to study vortex dynamics subject to externally imposed flows," AIP Conf. Proc. **1928**, 020007 (2018).
[48]C. A. F. Fracassi, R. Pakter, and Y. Levin, "Linear and non-linear instabilities of Kirchhoff's elliptical vortices," J. Stat. Mech. **2020**, 083205.
[49]N. J. Balmforth, S. G. L. Smith, and W. R. Young, "Disturbing vortices," J. Fluid Mech. **426**, 95 (2001).